

EFFECTIVE RESISTANCE OF GROUNDED HUMANS FOR WHOLE-BODY AVERAGED SAR ESTIMATION AT RESONANCE FREQUENCIES

K. Yanase and A. Hirata*

Nagoya Institute of Technology, 466-8555 Nagoya, Japan

Abstract—Whole-body averaged specific absorption rate (WBA-SAR) is used as a metric for human protection from whole-body exposures. The frequency at which the WBA-SAR becomes maximal is called “resonance frequency”. The present study proposes a scheme to estimate WBA-SAR at the resonance frequency based on an analogy between a human and a quarter-wavelength monopole antenna. Specifically, WBA-SAR can be estimated with the human body resistance once ankle current was obtained. Thus, it is essential to investigate the effective resistance for anatomically-based human models. Then, the effective resistances for different humans grounded on the perfect conductor are calculated to clarify the variability. The main factors for the variability were attributed to the body shape and model anatomy. In particular, WBA-SARs in human models grounded are found to be estimated from their BMI and respective measured ankle current in realistic environment, including a scenario of multiple wave exposure.

1. INTRODUCTION

There has been increasing public concern about the adverse health effects of human body exposure to electromagnetic waves. According to the international guidelines/standards [1, 2], whole-body average specific absorption rate (WBA-SAR) is used as a metric of basic restriction for radio frequency whole-body exposure. Thus, many studies have been reported for SAR evaluation (e.g., [3–7]). It is well known that the WBA-SAR largely depends on the frequency for exposure at the same incident power density [8–11]. Human height at the resonance frequency was shown to be approximately

Received 25 August 2011, Accepted 29 September 2011, Scheduled 4 October 2011

* Corresponding author: Akimasa Hirata (ahirata@nitech.ac.jp).

0.2 wavelengths of radio-frequency waves in free space for a lossy cylinder [12]. This relationship has been explained in analogy of quarter-wavelength monopole antenna and human [12]. The resonance frequency for grounded adults is a few dozen megahertz [10–18] and several dozen megahertz for children [11, 14, 16, 17, 18]. This frequency bands are assigned for FM/television broadcasting.

WBA-SARs for human models even in free space have been reported to be comparable to the basic restriction under the exposure at the reference level or allowable incident power density [1, 2]. WBA-SARs for a grounded human were larger than that of ungrounded human [10, 11]. Thus, attention has been paid to the SAR compliance for grounded human. In addition, WBA-SAR in the child models was larger than that of the adult at least in free space [13, 14, 19].

There are some attempts to estimate the ankle current of grounded humans for the compliance of safety standards [9, 18]. These studies are based on the analogy of human body and quarter-wave monopole antenna as mentioned above. In addition, the human body was simplified as a lossy cylinder. By extending the concept of the similarity between the human body and monopole antenna at respective resonance frequencies, WBA-SAR may be estimated with the human body resistance at the resonance frequency and the ankle current. The ankle current of human models can be measured easily [20]. Thus, the effective resistance for realistic models should be discussed for far-field exposure.

The purpose of the present study is to investigate the human body resistance and then to discuss its variability for different body models. Based on the finding, some insight to simplify the SAR compliance procedures will be given.

2. MODEL AND METHODS

2.1. Anatomically-based Human Model

MRI-based whole-body voxel models for different ages, genders, and races are considered; Japanese adult male (TARO) and female (HANAKO), together with child models of three, five, and seven years of old [21, 22]. A pregnant woman based on HANAKO is also considered [23]. A standardized European adult male (NORMAN) [12], female (NAOMI) [15] and American adult male models (BAFB) [24] are considered, together with those developed via international project; Virtual Family (Duke, Ella, Billie, and Thelionius) [25]. These models have the resolution of a few millimeters and are segmented into several dozen anatomical regions.

2.2. Computational Methods and Conditions

The finite-different time-domain (FDTD) method was used to calculate the electromagnetic power absorbed in the human models [26]. For geometries in which the wave-object interaction has to be considered in open region, the computational space has to be truncated by absorbing boundaries. We adopt perfectly matched layers (PML) as the absorbing boundaries, because this offers the advantages of very low reflections and relatively low computational costs. The thickness of the perfectly matched layer is chosen as 12 cells. The maximum conductivity of the layers was determined so that it has an attenuation of 40 dB for the normal incident to the layers. Our FDTD code has been validated through intercomaparison [27]; the difference of WBA-SARs between ours and those obtained at two different institutes were a few percents or less at the resonance frequencies.

The computational condition was shown in Figure 1. Either of the models was located on the ground plane. The separation between the human model and PML was maintained at 100 mm (50 cells). As an incident wave, a plane wave with a vertical polarization was considered. The reason for choosing this polarization is that the WBA-SAR becomes maximal due to a standing wave over the human body [11]. The incident power density was 2 W/m^2 . The frequency chosen is respective resonance frequency for each model. The respective resonance frequency for each model is listed in Table 1. The angle of incidence θ was 0° .

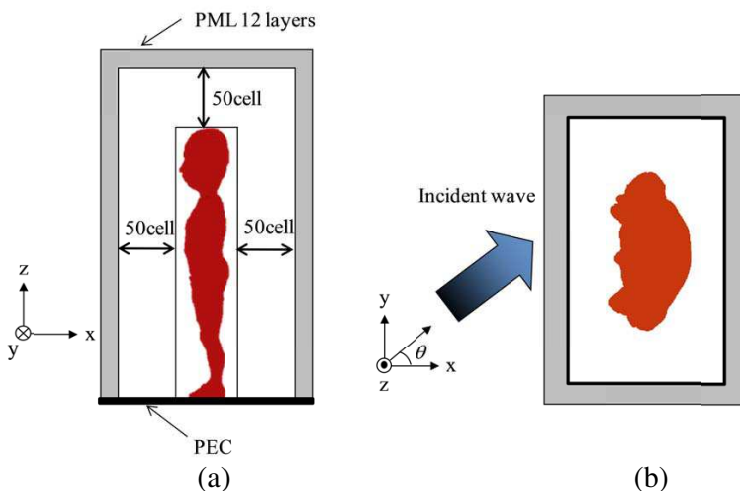


Figure 1. (a) The side and (b) top views of computational condition.

Table 1. The respective resonance frequency in (a) Japanese models and (b) European and American models.

(a)							
Models	TARO	7 years	5 years	3 years	HANAKO	pregnant -woman	
Resonance Frequency [MHz]	39	61	73	85	45	46	
(b)							
Models	Duke	Ella	Billie	Thelonious	NORMAN	NAOMI	BAFB
Resonance Frequency [MHz]	40	42	51	66	40	48	38

The dielectric properties of tissues are taken from [28]. When considering homogeneous human models, the dielectric properties of 2/3 that of muscle were used. Note that the human body is comprised of high and low water content tissues with the ratio of 2:1. The dielectric properties of low-water-content tissues, such as fat and bone, are much smaller than those of high-water-content tissues, such as muscle. Therefore, the dielectric properties of 2/3 that of muscle, which is a representative of high water content tissue, is often considered for fundamental discussion.

2.3. Review of Antenna Theory

This subsection reviews briefly some fundamental theory and definition of antenna toward deriving the effective resistance for grounded humans. The basic theory of this is based on the assumption that the human body grounded approximately considered as a quarter-wavelength monopole. Note that similar derivation has been given for a human body in free space.

Lets us summarize some definitions of antenna. For the current distribution on the antenna $I(z)$ and the maximum current I_o [A], the effective height of the antenna L_e [m] is given by the following equation:

$$L_e = \frac{1}{I_o} \int_0^L I(z) dz, \quad (1)$$

where L [m] is the physical height of the antenna.

The power received by the antenna P is given by the following

equation:

$$P = \frac{R^2 + X^2}{R} I_a^2 \tag{2}$$

where R and X are resistance and reactance of the grounded human, and I_a is the current. Note that $(R^2 + X^2)/R$ is considered as an equivalent resistance since the reactance X is approximately nonexistent at the resonance frequency. P corresponds to the power absorbed in the human body model.

3. COMPUTATIONAL RESULTS

3.1. Behavior of Human Models as Monopole at Their Respective Resonance Frequencies

The power absorption in the human body grounded would be considered in analogy with a quarter-wavelength monopole [9]. In order to verify this hypothesis for anatomically-based human models, the vertical conduction currents in the Japanese body models are shown in Figure 2. The vertical conduction current was obtained by integrating FDTD-derived conduction current density along the vertical axis over each horizontal plane. As shown in Figure 2, the current distributions of the Japanese models are similar to that of the quarter-wavelength monopole. Although not shown here, the distribution for the remaining models are also similar to one another.

Figure 3 shows the relationship between the human height H [m] and effective height H_e [m]. The effective heights for different models are calculated with (1) for the distributions shown in Figure 2. As shown in Figure 3, the strong correlation was obtained between the human height H [m] and effective height H_e [m]. Using the least

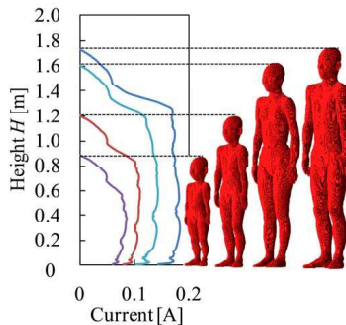


Figure 2. Vertical conduction current in the Japanese models.

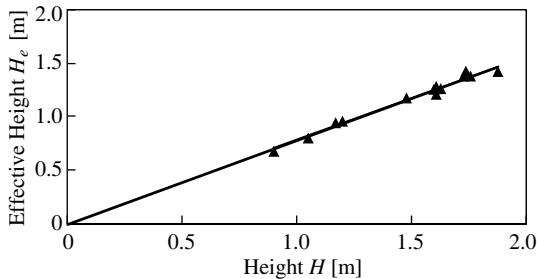


Figure 3. Relationship between human height and effective height for different human models.

squares method, the coefficient of determination was 0.982, suggesting that the human body models behave like antennas similar to one another despite of different shapes. The coefficient of the regression line was 0.783 for all the human models considered herein. Note that the less the calculated values depart from the regression line, the closer to unity the coefficient of determination is. This result suggested that the above-mentioned hypothesis was reasonably valid.

3.2. Effective Resistance for Cylinder

In order to discuss the variability of effective resistance, we considered the effective resistance of lossy cylinder, since it has been used for the SAR compliance by virtue of light weight and the simplicity of fabrication [20]. It is well known that the lumped resistance is given by the following equation:

$$R = \frac{1}{\sigma} \times \frac{L}{S} \quad (3)$$

where R [Ω] is resistance, σ [S/m] is conductivity, S [m^2] is cross-sectional area, and L [m] is the length of cylinder. Note that the weight of cylinder comprised of biological tissue W [kg] is given approximately by the following equation:

$$W = \rho \times H \times S \quad (4)$$

where ρ [kg/m^3] is volume density and H [m] is human height. From (3) and (4), the following equation can be obtained:

$$R = \frac{\rho}{\sigma} \times \frac{H^2}{W} = \frac{\rho}{\sigma} \times \frac{1}{\text{BMI}} \quad (5)$$

where $\text{BMI} = W/H^2$. From (5), the effective resistance is inversely proportional to BMI (body-mass index). There are the two main

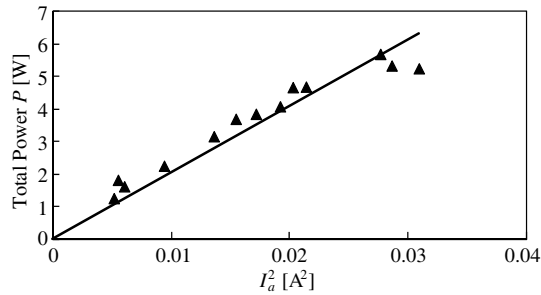


Figure 4. Relationship between ankle current and power absorption for different human models.

differences between the human body and cylinder. One is the model shape and the other is the model anatomy or the spatially-dependent dielectric property. From the latter factor, the displacement current may not be ignored, as can be seen from Figure 1.

3.3. Effective Resistance for Anatomically-based Models

The relationship between the human body resistance and ankle current has been investigated for different human models. As shown in Figure 4, strong correlation was observed between the absorbed power P and the square of the ankle current I_a . With the least squares method the relationship is characterized in the following equation:

$$P = 204.4I_a^2 \quad (6)$$

where the coefficient of determination was 0.890. From (6), the average value of the effective resistance for the grounded human was 204.4Ω . To discuss the effect of the model inhomogeneity, the effective resistance for homogeneous model is calculated. The average value for the homogenized models was 127.5Ω , which was 37% smaller than those of the anatomically-based models. This difference is attributed to the model inhomogeneity. The dominant tissue in the cross sectional area at the height of the ankle is the bone whose conductivity is low. Thus the current at the ankle of the anatomically-based models grounded results in smaller ankle current, as shown in Figure 2. For comparison, the effective resistance for a cylinder is also calculated. The height and weight of the cylinder were chosen so as to coincide with those of TARO. The effective resistance of the cylinder was calculated as 63Ω , which is comparable to the that reported in [9]. The point to be stressed here is that the value estimated from the cylinder is smaller than that of homogenized TARO of 122Ω . In other words, the model shape is also a determinative factor of the resistance.

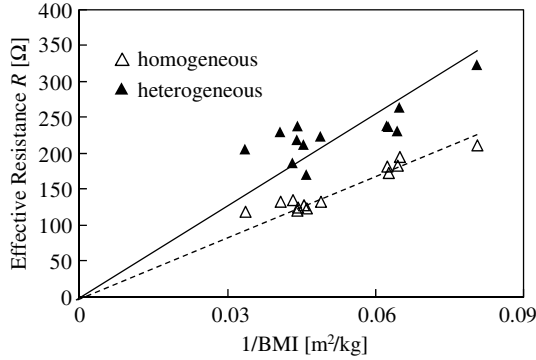


Figure 5. Relationship between the reciprocal of the BMI and effective resistance for anatomically-based models and their homogenized models on the ground.

Table 2. The respective effective resistance in (a) Japanese models and (b) European and American models.

(a)							
Models	TARO	7years	5years	3years	HANAKO	pregnant -woman	
Effective Resistance [Ω]	169	237	264	238	223	212	
(b)							
Models	Duke	Ella	Billie	Thelonious	NORMAN	NAOMI	BAFB
Effective Resistance [Ω]	186	218	231	324	230	238	205

Figure 5 shows the relationship between the reciprocal of the BMI and effective resistance for anatomically-based models, their homogeneous models. From Figure 5, the regression line obtained using the least squares method was presented as follows:

$$P = 4249/\text{BMI} \times I_a^2 \quad (7)$$

3.4. Discussion on Variability of Human Body Resistance

The effective resistances for the heterogeneous models were larger than those of their homogenized models. The point to be stressed here is

that the difference caused by the model inhomogeneity is 50%. The average differences for each plot from regression line for anatomical and their homogenized models were 15% and 6%, respectively (see Figure 5). Thus, the model inhomogeneity causes the variation of effective resistance of 9%, in addition to that caused by the model shape of 6%.

The respective effective resistances for the human models calculated from (2) are listed in Table 2. As seen from Table 2, the respective effective resistance varied in the range between 169Ω and 324Ω . The main factor for the variability is body shape, which is characterized by BMI. It is known that there is correlation between age and BMI [29]. The age dependency of the effective resistance for grounded human is shown in Figure 6, together with the average and the 95% confidence interval of reciprocal BMI for Equation (7). As seen from Figure 5, the effective resistances for grounded human considered herein are within the 95% confidence interval of reciprocal BMI, confirming the effectiveness of Equation (7).

3.5. Verification for Multiple Wave Exposures

In order to verify the effectiveness of our proposal for multiple wave exposures [30], the ankle current and WBA-SAR are calculated for Japanese child model of three years old exposed to two plane waves at

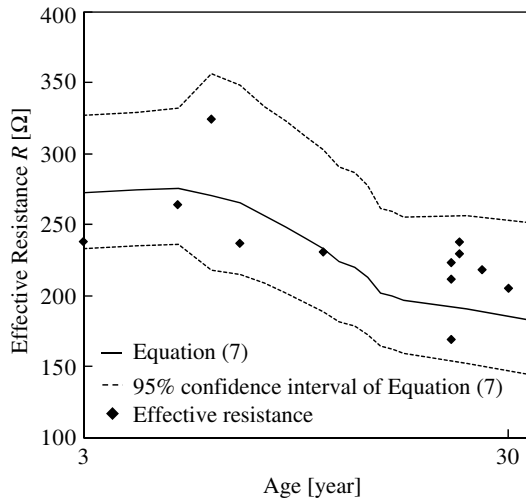


Figure 6. Age dependence of the effective resistance for grounded humans.

85 MHz. The angles of incidence θ are 0 and 60° . The incident power densities are chosen as 2 W/m^2 and 1 W/m^2 , respectively. Note that the effect of angle of incidence on SAR is discussed elsewhere (e.g., [31, 32]). WBA-SAR were estimated as 0.269 W/kg from the computed ankle current of 0.12 A and the effective resistance of 238Ω computed in the above section. The FDTD-derived WBA-SAR was 0.268 W/kg . This comparison suggests the effectiveness of our proposal even for multiple wave exposures.

4. SUMMARY

In the present study, the effective resistances of grounded human models are investigated at their respective resonance frequencies. The motivation of this investigation was that the WBA-SARs of humans grounded were close to the basic restriction or the limit in the safety guidelines/standards [1, 2]. From our computation, the effective resistances for grounded humans were in the range between 170Ω and 324Ω . The main factor for this variability was body shape, which was characterized by BMI. The other factor could be attributed to the model inhomogeneity. Its effect on the body resistance was 50%. Thus, a previous approach with the cylinder [9] was suggested to cause significant difference compared to the case using realistic humans. This finding would be valuable for further improvement of the physical phantom used for SAR compliance [20].

From (6), we can estimate WBA-SAR in the human models grounded from BMI and measured ankle current in realistic environments, even though the respective resonant frequencies are different for different human models. This finding may be useful for further consideration of safety guidelines/standards and compliance of WBA-SAR in realistic electromagnetic environments, including multiple wave exposures.

Future work is to conduct measurement to verify the relationship between human body resistance and BMI.

ACKNOWLEDGMENT

This work was supported in part by Grant-in-Aid for Young Scientists (B) 21760257. The authors would like to thank Drs. Soichi Watanabe and Tomoaki Nagaoka for providing the models of Japanese child.

REFERENCES

1. ICNIRP (International Commission on Non-Ionizing Radiation Protection), "Guideline for limiting exposure to time-varying electric, magnetic, and electromagnetic fields (up to 300 GHz)," *Health Phys.*, Vol. 74, 494–522, 1998.
2. IEEE Standard for Safety Levels with Respect to Human Exposure to Radio Frequency Electromagnetic Field, 3 kHz to 300 GHz (C95.1), 2005.
3. Sabbah, A. I., N. I. Dib, and M. A. Al-Nimr, "SAR and temperature elevation in a multi-layered human head model due to an obliquely incident plane wave," *Progress In Electromagnetics Research M*, Vol. 13, 95–108, 2010.
4. Omar, A. A., "Complex image solution of SAR inside a human head illuminated by a finite-length dipole," *Progress In Electromagnetics Research B*, Vol. 24, 223–239, 2010.
5. Liu, Y., Z. Liang, and Z. Yang, "Computation of electromagnetic dosimetry for human body using parallel FDTD algorithm combined with interpolation technique," *Progress In Electromagnetic Research*, Vol. 82, 95–107, 2008.
6. Mohsin, S. A., N. M. Sheikh, and U. Saeed, "MRI induced heating of deep brain stimulation leads: Effect of the air-tissue interface," *Progress In Electromagnetics Research*, Vol. 83, 81–91, 2008.
7. Lopez-Martin, E., J. C. Bregains, F. J. Jorge-Barreiro, J. L. Sebastián-Franco, E. Moreno-Piquero, and F. Ares-Pena, "An experimental set-up for measurement of the power absorbed from 900 MHz GSM standing waves by small animals, illustrated by application to picrotoxin-treated rats," *Progress In Electromagnetics Research*, Vol. 87, 149–165, 2008.
8. Hirata, A., H. Sugiyama, and O. Fujiwara, "Estimation of core temperature elevation in humans and animals for whole-body averaged SAR," *Progress In Electromagnetics Research*, Vol. 99, 53–70, 2009.
9. Korniewicz, H., "The first resonance of a rounded human being exposed to electric field," *IEEE Trans. Electromagnet. Compat.*, Vol. 37, No. 2, 296–299, 1995.
10. Durney, C. H., "Electromagnetic dosimetry for models of humans and animals: A review of theoretical and numerical techniques," *Proc. IEEE*, Vol. 68, 33–40, 1980.
11. Gandhi, O. P., "State of knowledge for electromagnetic absorbed dose in man and animals," *Proc. IEEE*, Vol. 68, 24–32, 1980.

12. Dimbylow, P. J., "FDTD calculations of the whole-body average SAR in an anatomically realistic voxel model of the human body from 1 MHz to 1 GHz," *Phys. Med. Biol.*, Vol. 42, 479–490, 1997.
13. Dimbylow, P. J., "Fine resolution calculations of SAR in the human body for frequencies up to 3 GHz," *Phys. Med. Biol.*, Vol. 47, 2835–2846, 2002.
14. Wang, J., S. Kodera, O. Fujiwara, and S. Watanabe, "FDTD calculation of whole-body average SAR in adult and child models for frequencies from 30 MHz to 3 GHz," *Phys. Med. Biol.*, Vol. 51, 4119–4127, 2006.
15. Dimbylow, P., "Resonance behavior of whole-body average specific absorption rate (SAR) in the female voxel models, NAOMI," *Phys. Med. Biol.*, Vol. 50, 4053–4063, 2005.
16. Conil, E., A. Hadjem, F. Lacroux, M. F. Wong, and J. Wiart, "Variability analysis of SAR from 20 MHz to 2.4 GHz for different adult and child models using finite-difference time-domain," *Phys. Med. Biol.*, Vol. 53, 1511–1525, 2008.
17. Dimbylow, P. and W. Bolch, "Whole-body-averaged SAR from 50 MHz to 4 GHz in the University of Florida child voxel phantoms," *Phys. Med. Biol.*, Vol. 52, 6639–6649, 2007.
18. Hirata, A., K. Yanase, O. Fujiwara, A. Y. Simba, T. Arima, and S. Watanabe, "Estimation of whole-body averaged SAR of grounded human at resonance frequency from ankle current of simplified phantom," *Proc. EMC Europe, O-Tu.D1*, 2011.
19. Zhang, M. and A. Alden, "Calculation of whole-body SAR from a 100 MHz dipole antenna," *Progress In Electromagnetics Research*, Vol. 119, 133–153, 2011.
20. Takahashi, Y., T. Arima, P. Pongpaibool, S. Watanabe, and T. Uno, "Development of a liquid-type human-body equivalent antenna using NaCl solution," *Int'l Zurich Symp. Electromagnet. Compat.*, BIO2-5, Sep. 2007.
21. Nagaoka, T., S. Watanabe, K. Sakurai, E. Kunieda, S. Watanabe, M. Taki, and Y. Yamanaka, "Development of realistic high-resolution whole-body voxel models of Japanese adult males and females of average height and weight, and application of models to radio-frequency electromagnetic-field dosimetry," *Phys. Med. Biol.*, Vol. 49, 1–15, 2004.
22. Nagaoka, T., E. Kunieda, and S. Watanabe, "Proportion-corrected scaled voxel models for Japanese children and their application to the numerical dosimetry of specific absorption rate for frequencies from 30 MHz to 3 GHz," *Phys. Med. Biol.*, Vol. 52, 6695–6711, 2008.

23. Nagaoka, T., T. Togashi, K. Saito, M. Takahashi, K. Ito, and S. Watanabe, "An anatomically realistic whole-body pregnant-woman model and specific absorption rates for pregnant-woman exposure to electromagnetic plane waves from 10 MHz to 2 GHz," *Phys. Med. Biol.*, Vol. 52, 6731–6745, 2007.
24. Mason, P. A., W. D. Hurt, T. J. Walter, A. D'Amdrea, P. Gajsek, K. L. Ryan, D. A. Nelson, K. I. Smith, and J. M. Ziriak, "Effects of frequency, permittivity and voxel size on predicted specific absorption rate values in biological tissue during electromagnetic-field exposure" *IEEE Trans. Microwave Theory Tech.*, Vol. 48, No. 11, 2050–2058, 2000.
25. Christ, A., W. Kainz, E. G. Hahn, K. Honegger, M. Zefferer, E. Neufeld, W. Rascher, R. Janka, W. Bautz, J. Chen, B. Keifer, P. Schmit, H. P. Hollenbach, J. Shen, M. Oberle, D. Szczerba, A. Kam, J. W. Guag, and N. Kuster, "The Virtual Family — development of surface — based on anatomical methods of two adults and two children for dosimetric simulations," *Phys. Med. Biol.*, Vol. 55, 22–38, 2010.
26. Taflove, A. and S. Hagness, *Computational Electrodynamics: The Finite-difference Time-domain Method*, 3rd edition, Artech House Publishers, Norwood, MA, 2003.
27. Dimbylow, P. J., A. Hirata, and T. Nagaoka, "Intercomparison of whole-body averaged SAR in European and Japanese voxel phantom," *Phys. Med. Biol.*, Vol. 53, 5883–5898, 2008.
28. Gabriel, C., "Compilation of the dielectric properties of body tissues at RF and microwave frequencies," *Brooks Air Force Technical Report*, AL/OE-TR-1996-0037, 1996.
29. Penman, A. D. and W. D. Johnson, "The changing shape of the body mass index distribution curve in the population: Implications for public health policy to reduce the prevalence of adult obesity," *Prev. Chronic Dis.*, Vol. 3, No. 3, A74, 2006.
30. Conil, E., A. Hadjem, A. El Habachi, and J. Wiart, "Whole body exposure at 2100 MHz induced by plane wave of random incidences in a population," *Comptes Rendus Phys.*, Vol. 11, 531–540, 2010.
31. Conil, E., A. Hadjem, A. Gati, M.-F. Wong, and J. Wiart, "Influence of plane-wave incidence angle on whole body and local exposure at 2100 MHz," *IEEE Trans. Electromagnet. Compat.*, Vol. 53, No. 1, 48–52, 2011.
32. Hirata, A., H. Watanabe, and T. Shiozawa, "SAR and temperature rise in the human eye induced by obliquely incident plane waves," *IEEE Trans. Electromagnet. Compat.*, Vol. 44, No. 4, 594–596, Nov. 2002.